Millimeter-Wave Substrate Integrated Gap Waveguide Leaky-Wave Antenna for WiGig Applications

Mohammad Reza Rahimi, *Student Member*, IEEE, Nima Bayat-Makou, *Member*, IEEE, and Ahmed A. Kishk, *Fellow*, IEEE

***Abstract*—A new design of an H-polarized leaky-wave antenna (LWA) based on the substrate integrated gap waveguide (SIGW) technology is introduced. The antenna shows a good scanning capability from backward to a near broadside direction (from – 36° to – 15°) with a peak gain of 17.67 dBi within 1.3 dB variation over 57-64 GHz and wide impedance bandwidth. A pair of the LWAs is parallelly excited through a Y-power divider and terminated with the other end in series providing an additional 3 dB gain compared to the single LWA. Both designs show over 88% radiation efficiency and over 86% total efficiency. The fabricated prototypes of both antennas are made of multi-layered PCB technology. The measurement results are showing good agreement with the simulations.**

***Index Terms*—Ridge gap waveguide (RGW); leaky-wave antenna (LWA).**

I. Introduction

The millimeter-wave (30 to 300 GHz) considered as an undeveloped band of the radio frequency (RF) spectrum can provide high-speed wireless broadband communications of more than 10 Gbits/s [1], [2]. The recently introduced wireless gigabit (WiGig) specification enables the communication devices to deliver high-performance wireless data over the unlicensed 60 GHz frequency band, known as the industrial, scientific and medical (ISM) band, which covers the range of 57-64 GHz [3].

Considerable effort has been made to design microwave components for the millimeter wave (mm-Wave) frequencies. The conventional well-characterized planar transmission lines such as microstrip (MS) line and coplanar waveguide (CPW) have been widely utilized in a variety of RF components, but the power leakage due to surface waves in the dielectric substrate causes serious crosstalk and interference problems on various printed circuit transmission lines. Therefore, there has been a necessity for re-thinking in RF design techniques to reach a technology with improved electrical performances, flexible manufacturing and self-packaging capabilities with affordable cost.

Manuscript received October 19, 2018; revised December 3, 2018; accepted April 3, 2019. (*Corresponding author: Mohammad Reza Rahimi.)*

M. R. Rahimi and N. Bayat-Makou are with the Poly-Grames Research Center, Polytechnique Montreal, University of Montreal, Montreal, QC H3T 1J4, Canada (e-mail: Mohammad-reza.rahimi@polymtl.ca, nima.bayat-makou@polymtl.ca).

A. A. Kishk is with the Department of Electrical and Computer Engineering, Concordia University, Montreal, QC H3G 1M8, Canada (e-mail: kishk@encs.concordia.ca).

Color versions of one or more of the figures in this paper are available online at http://ieeexplore.ieee.org. Digital Object Identifier

The ridge gap waveguide technology (RGW) has been introduced in [4] and [5] as a new guiding structure for millimeter waves, which is an extension to the soft surface concept [6]. The ideal RGW configuration is guiding medium between two parallel perfect electric conductors (PEC/PEC) surrounded from both sides by a PEC and perfect magnetic conductor (PMC) separated by a gap less than $\lambda_g/4$. As the PMC is not available in nature, it is replaced by an artificial magnetic conductor (AMC) over a specific bandwidth, which was realized by a texture of bed of nails in [7] of height $\lambda_g/4$ that suppress the propagation outside the guiding medium. The groove gap waveguide introduced in [8] is another configuration of gap waveguide that avoids the electrical contacts and shows higher Q factor than the ridge gap waveguide. But, the resonant length of them can be affected by the tolerance on the position of pin walls compare to the rectangular waveguide that has higher Q_s. The printed version of this technology also known as printed ridge gap waveguide (PRGW) was developed in [9] in which the AMC surfaces was realized by printed mushroom surfaces. Ensuring a uniform thin air gap for the PRGW at millimeter waves has become problematic for the large structures. So, the gap height was filled with a thin low loss and a low dielectric constant substrate to guarantee the fixed gap height between the PEC and AMC layers in the substrate integrated gap waveguide (SIGW) configuration introduced in [10].

In recent years, the fan beam radiation pattern has received considerable attention at mm-wave frequencies for the short-range radar systems detection [11] or image processing applications [12]. The fan beam was also used with the Luneberg lens as a feed of high gain reflector antenna at the millimeter frequencies [13]. Leaky wave antenna (LWA) as a member of the traveling wave antenna family [14] has the ability to produce a fan beam radiation pattern [15]. The LWA has been widely considered among antenna engineers because of its advantages over the slot array and phased array antennas [16]. It can efficiently deliver a scanning beam without any need for phase shifters, and its radiating elements can be conveniently excited without deploying a complicated feeding network as used in the regular array antennas; so that they are of low-cost fabrication. The standing wave-excited slot arrays, such as the ones in [17] and [18], the scan range is limited due to the resonant nature of the narrow slots (frequency dependent slot). On the other hand, a metamaterial-based LWA can achieve a wide scanning range easily [19]-[21], but it adds more complexity to the antenna in the millimeter-wave band. The conventional planar LWAs are enduring relatively significant gain variation over the scanning range [22]-[25], which would deteriorate when those structures scaled to the high-frequency regime. For instance, the unit cell geometry of microstrip LWA in [26] is loaded with capacitive and inductive radiating elements, which

enable the LWA to preserve its gain while scanning through broadside. However, because of microstrip geometry of the LWA, it cannot produce the same gain performance if it is designed to be used at mm-wave frequencies.

Here, two designs of planar LWAs are presented based on the SIGW technology, which provides a reliable self-packaged and low loss guiding medium at mm-wave with less dispersive propagation characteristics. The antennas operating frequency band is tuned for the WiGig specifications. The first design is a 1D-periodic LWA, which has a low profile, low side lobe level, high radiation efficiency, and an almost stable gain over the scanning bandwidth. The second antenna is a 2×1 array of the first design, which shows a 3 dB gain higher than the single LWA with high radiation efficiency. The prototypes are fabricated on two-layer substrates and excited by a transition from the MS line to the SIGW.

The paper is organized as follows. In section II, the configuration of SIGW, which is used in the LWA design is elaborated. Its periodic structure analysis is given to determine its stopband features. In section III, the slot-array design and the antenna characteristics are discussed. Section IV describes the antenna matching issues based on the newly designed transitions. In section V and VI, the simulated and measured results of the single SIGW-LWA arm and the dual-arm array design are presented. Finally, conclusions and discussions are given in section VII.

II. SIGW Design Configuration

At the desired operating band, a mushroom unit cell including a grounded superstrate for the SIGW periodic structure has to be designed, which provides the required stopband. The unit cell structure and its dispersion diagram are shown in Fig. 1. The printed SIGW mushroom unit cell has a rectangular patch grounded by a plated via and covered by a dielectric substrate, which is topped by a conductor. Rogers RT5880 substrate with the dielectric constant of 2.2 is used for the upper layer, and Rogers RT6002 with the dielectric constant of 2.94 is used for the lower layer. The factors that affect the band gap provided by the periodic structure of the unit cell are the layer thicknesses, periodicity, and mushroom dimensions. A detailed study to investigate these factors can be found in [27]. The band gap of the designed cell is from 31.4 to 70.8 GHz. To show the guiding characteristics of the SIGW, a single line of SIGW surrounded from both sides by three rows of cells is considered. It is enough to study a single transverse segment of SIGW line, as a waveguide cell with only longitudinal periodic boundary conditions to extract the structure, dispersion relation, as shown in Fig. 2. To suppress any the possible leakage of the waves under the ridge, a single row of metallic via is located under the printed ridge to ground the ridgeline. The thin substrate filling the gap height is holding the upper conducting plate over the structure. The dispersion diagram of the SIGW line is shown in Fig. 3 showing the single quasi-TEM propagating mode along the ridge in the stopband of the periodic structure. The cutoff region provided by the AMC-PEC parallel plate decays the fields outside of the guiding region. The width of the ridgeline is tuned for a 50 Ω characteristic impedance with a single propagating mode between 32.3-67.8 GHz. A detailed study on how to extract the characteristic impedance can be found in [28].

III. SIGW-LWA Design

As known, the wavenumber of the physical fast wave radiating in 1D-periodic LWA is a complex number,

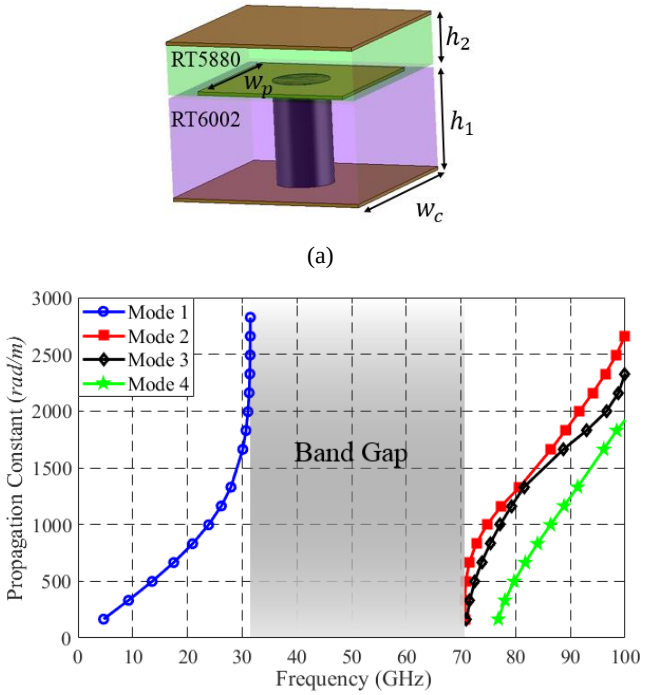

Fig. 1. (a) Unit cell dimensions h_1 = 0.508, h_2 = 0.254, w_p = 0.819, w_c = 1.05 (dimensions are in mm), and (b) Dispersion diagram of the unit cell.

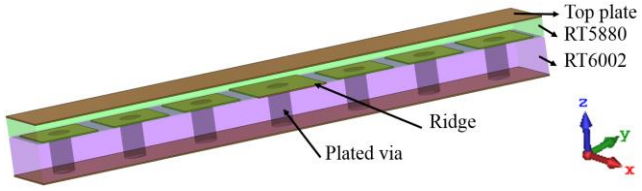

Fig. 2. Layers configuration of the SIGW transverse cell.

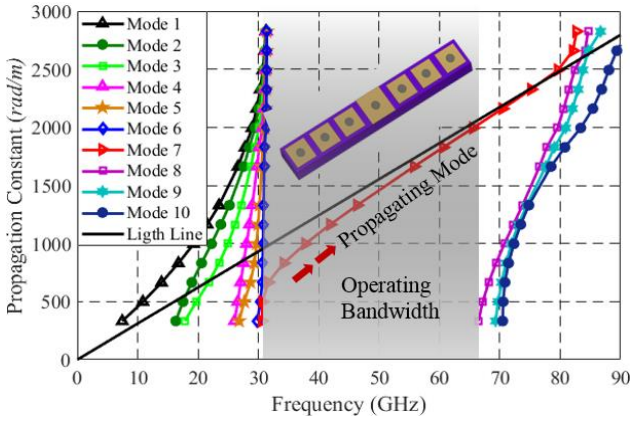

Fig. 3. Dispersion diagram of the SIGW line.

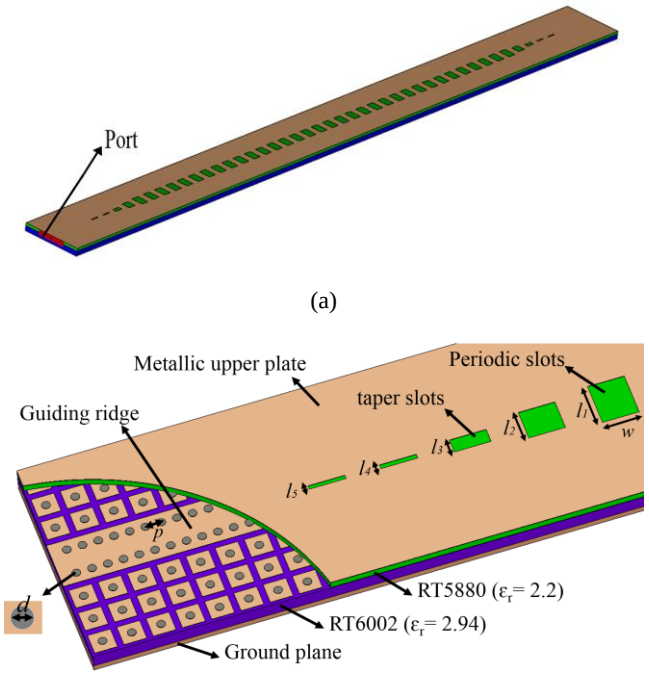

Fig. 4. Configuration of the SIGW-LWA with d = 0.3 mm, p = 0.56 mm, w = 1.32 mm, l_1= 1.67 mm, l_2 = 1.18 mm, l_3 = 0.52 mm, l_4 = 0.18 mm, l_5 = 0.15 mm., (a) 3D view of the whole structure, and (b) A zooming close with part of the upper substrate removed.

including propagation constant β as the real part and attenuation constant α as the imaginary part given as:

$$k_{zn} = \beta - j\alpha \tag{1}$$

The propagation constant controls the beam angle and the attenuation constant controls the beam width, which represents the losses and leakage ratio (α/k_0). The large leakage per unit length in LWA, which is showing a large leakage ratio, results in short effective aperture and consequently a wide beamwidth. Small leakage per unit length provides a long effective aperture and a narrow beam. The periodicity of the slot-array or strips causes infinite space harmonics, which are characterized by β_n. The dominant mode for the periodic LWA is slow wave ($\beta > k_0$), which is not a radiating mode. However, the radiation pattern of the 1D-periodic LWAs is usually due to n = -1 space harmonic, which is a physical fast wave ($|\beta_{-1}/k_0|<1$) for a specific frequency range with a complex wavenumber. In this kind of LWAs, the main beam direction is related to the first space harmonic (β_{-1}). The equations below show the relationship between the propagation constant of a periodic LWA, the beam direction (θ_m), the period, p, and the free space wavenumber, k_0 where n is an integer.

$$\beta_n = \beta_0 + 2\pi n / p \tag{2}$$

$$\sin\theta_m = \beta_{-1} / k_0 \,. \tag{3}$$

The geometry of the SIGW-LWA is shown in Fig. 4, which consists of two layers of substrates. A periodic set of series centered transverse slots is applied on the top of the SIGW conducting plane parallel to the guiding ridge. According to [22], to control and minimize the unwanted end reflections, tapered slots are added to both ends that provide an ideal field in the uniform slots region. The initial SIGW-LWA structure is excited by a wave port provided by the simulator. The wave ports are extended almost one cell around the guiding ridge to capture all fringing fields on both sides of the ridge. By varying the frequency, the phase constant and the electrical length between the slots are varying, which causes a change in the progressive phase between the slots. Therefore, the angle of the main beam is scanning by varying the frequency. To design the slots of the SIGW-LWA, three steps are considered. In the first step, the slots periodicity is determined. As the operating frequency band for the WiGig applications is 57-64 GHz, the slots periodicity should be chosen to excite only the n = -1 space harmonic (β_{-1}) over this band. Fig. 5 shows the Brillouin diagram for a periodicity of p = 2.57 mm. According to this diagram, we have only one beam in the backward quadrant for the frequency range above 50 GHz due to the excitation of the n = -1 space harmonic. Second, the slot length design is considered and it is tunned to be 1.67 mm, which almost equal to the half of guided wavelength in the SIGW. To uniformly excite these periodic slots through the SIGW line, the width of the ridgeline should be slightly wider than the slot length. In the present design, the width of the propagating ridge under the periodic slots is fixed to be 1.9 mm. In the third step, the width of the periodic slots is tuned to reach a low and almost constant value of the attenuation constant over the band. Accordingly, we could obtain an approximately constant gain over the bandwidth due to the fixed amount of leakage per unit length. It should be mentioned that to decrease the effect of the fringing fields and to suppress any possible propagation under the guiding ridge, two rows of metallic vias are placed under the edge of the guiding ridgeline. The vias spacing and diameter are adjusted based on the conditions given in [29], which is $d/p > 0.5$, to have a minimum leakage of the waves under the ridgeline. According to [30] and [31], for a LWA with the leakage factor of $\alpha/k_0 < 0.02$, a length of $20\lambda_0$ is required to radiate more than 90% of the input power. Therefore, the length of the whole LWA including periodic section and tapered ends is fixed for this length. For the proper radiation, the slot length should be around half a guided wavelength ($\lambda_g/2$) while the

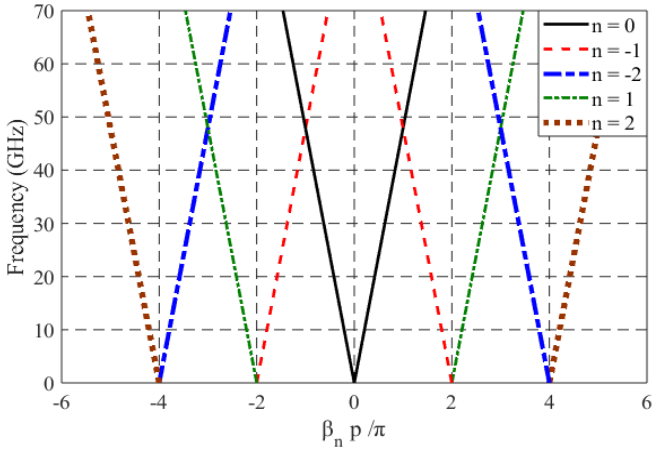

Fig. 5. Brillouin diagram for a periodicity of p = 2.57mm.

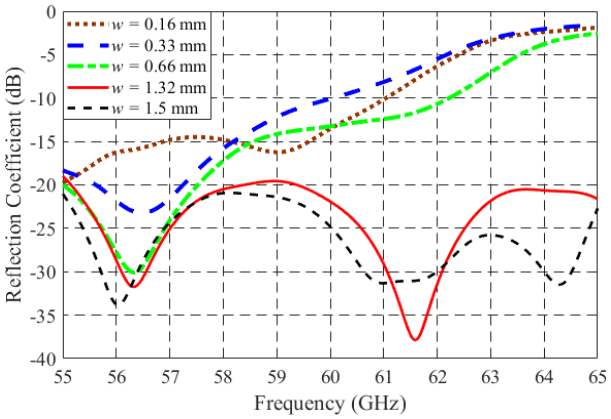

Fig. 6. Reflection coefficient for different width of slots.

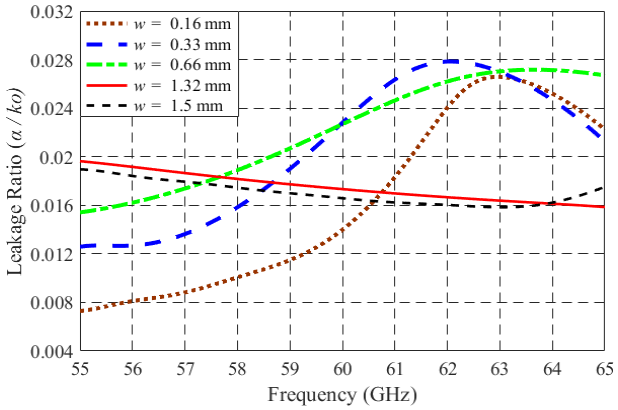

Fig. 7. Leakage ratio for different width of slots.

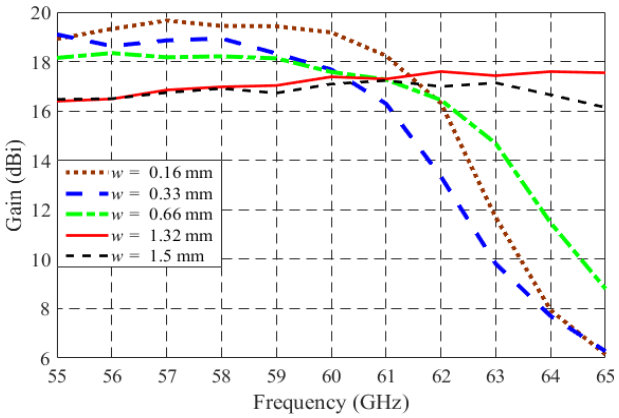

Fig.8. Realized gain for different width of the slots.

TABLE I
ANTENNA CHARACTERISTICS WITH DIFFERENT SLOT WIDTH

Slot width(mm)	Operating Frequency(GHz)	Bandwidth (%)	Scanning angle (degree)
0.16	46.9-61	23	-73 to -13
0.33	48.2-60	21.8	-63 to -12
0.66	49.1-62.2	23.5	-62 to -10
1.32	51.6-68	27.4	-62 to -5
1.5	51.9-66.1	24	-62 to -4

slot width should be w ≤ (0.05-0.1) λ_g [32]. Here, the analysis of different slot widths (0.05 λ_g - 0.45 λ_g) for the SIGW-LWA with the length of 20 λ_0 are performed. A parametric study is accomplished for the different widths of the periodic slots to evaluate the performance of the LWA in terms of the reflection coefficient, leakage ratio, and gain as illustrated in Fig. 6, Fig. 7, and Fig. 8, respectively. Table I provides the antenna characteristics for different slot width. Based on these analyses, it has been seen that the slot width of 1.32 mm results in the most suitable design providing a relatively stable gain, constant leakage ratio less than 0.02, and wider impedance bandwidth with a reflection coefficient less than -20 dB. Therefore, a narrow beam for the antenna radiation pattern is expected.

IV. Antenna Configuration with Transitions

As mentioned, the width of the ridgeline exciting the periodic slots is set to be 1.9 mm, which is corresponding to a characteristic impedance of 29 Ω. However, to excite the antenna through a standard connector for measurement purposes, it should be connected to a 50 Ω transmission line. Therefore, the designed LWA structure has to be matched to a

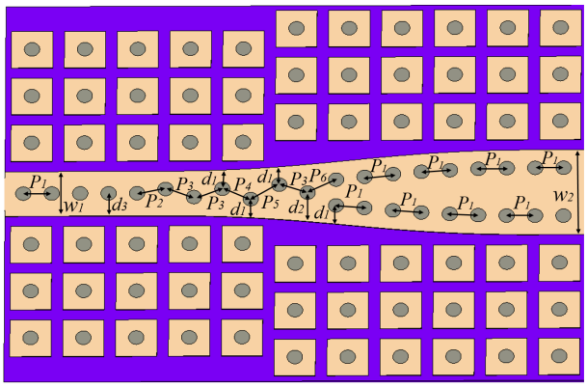

(a)

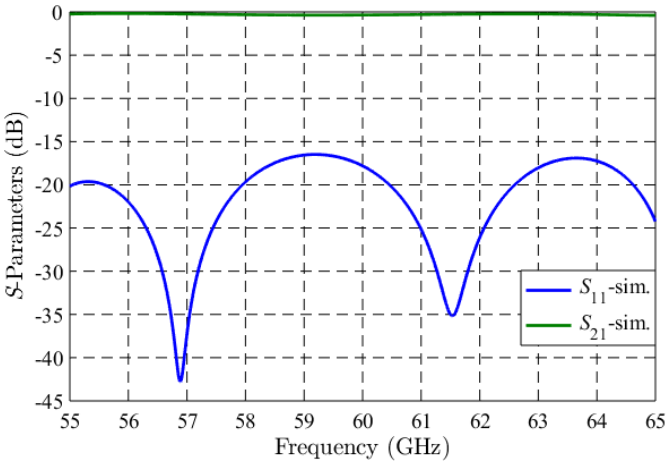

(b)

Fig. 9. (a) Tapered ridge transition of SIGW-LWA with d_1 = 0.26 mm, d_2 = 1.9 mm, d_3 = 0.37 mm, p_1 = 0.56 mm, p_2 = 0.57 mm, p_3 = 0.59 mm, p_4 = 0.62 mm, p_5 = 0.65 mm, p_6 = 0.63 mm, w_1 = 1 mm, and w_2 = 1.9 mm, and (b) Simulated *S*-parameters of the back-to-back transition.

50 Ω line. The PRGW structures can be easily excited by an MS line with the substrate thickness equal to the gap height of the PRGW [33]. Here, to excite this LWA, first, a tapered transition is applied to match the ridgeline of LWA to the 50 Ω SIGW line, as shown in Fig. 9 (a). The tapered transition is adjusted to cover the whole the frequency bandwidth. As seen from the transition geometry, two sets of parallel vias are used close to the ridge edge to suppress the possible leakage under the wide printed ridge. Along the tapered transition, the parallel vias are narrowed down to the single row under the 50 Ω SIGW line. Then, another transition is used to connect the 50 Ω SIGW to the 50 Ω MS line. The width of 50 Ω MS line is smaller than the width of 50 Ω SIGW line due to differences in the effective permittivity of propagating medium (width of MS is 0.74 mm and width of the guiding ridgeline is 1 mm). A detailed study of this transition is given in [34]. The simulated *S*-parameters of the back-to-back connection of transitions are plotted in Fig. 9 (b) showing a good insertion loss response. Fig. 10 shows the total configuration and the separated layers of the SIGW-LWA with the tapered transition and the MS line. The electric field distribution inside the antenna starting from the feeding MS line is shown in Fig. 11. The tapered transition provides a relatively uniform field of quasi-TEM propagation on the ridgeline exciting the periodic slots. The fabricated prototype of the LWA excited by end launch connectors is shown in Fig. 12. A 3D-printed holder is prepared to support the antenna safely during the measurement.

V. Simulated and Measured Results of SIGW-LWA

The simulated and measured *S*-parameters of the SIGW-LWA held by the 3D-printed base is shown in Fig. 13. The reflection coefficients are below -15 dB with good agreement between the simulation and measurement results. In Fig. 14, the measured and simulated leakage ratios show low values less than 0.02 ($\alpha/k_0 < 0.02$) that provides the LWA with a narrow beam and long effective aperture. Fig. 15 shows the realized gain of the co-polar E-plane radiation pattern for two frequencies at first and the end of the desired bandwidth (57 GHz and 64 GHz). Although there is a small discrepancy between the beam angle observed due to the shift in frequency, the measured radiation pattern is close to the simulated one. The measured peak gain of the antenna is 17.67 dBi with less than 1.3 dB variation and the beam scanning range is between –36˚ and –15˚ over the bandwidth. The backward radiating wave of this LWA is a physical proper fast wave, and the power flows inward radially, based on LWA analysis given in [35], [36]. In addition, the phase and group velocities are in the opposite directions, and the phase constant is negative ($\beta_{-1} < 0$) in the frequency range of 57-64 GHz. The cross-polar pattern of all frequencies in E-plane are below 30 dB from the main beam, and they are not shown in Fig. 15. This LWA has a narrow fan beam pattern due to the significant width of the antenna in the x-direction. Fig. 16 shows the 3D radiation pattern of SIGW-LWA at 64 GHz. For the main beam off the broadside direction (θ = 0°), the H-plane pattern measurement is difficult, based on our available facilities. Therefore, we trust the simulated result, which shows good agreement with E-plane measurements. It should be mentioned that the relatively wide width of the radiating slots has caused emerging a comparable cross-polarization in H-plane. Fig. 17 shows the simulated H-plane at three frequencies of the bandwidth for the different θ angles.

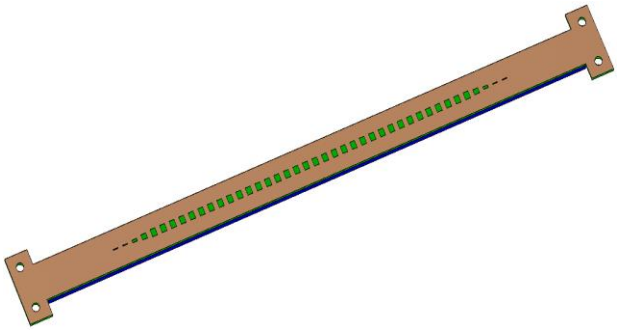

(a)

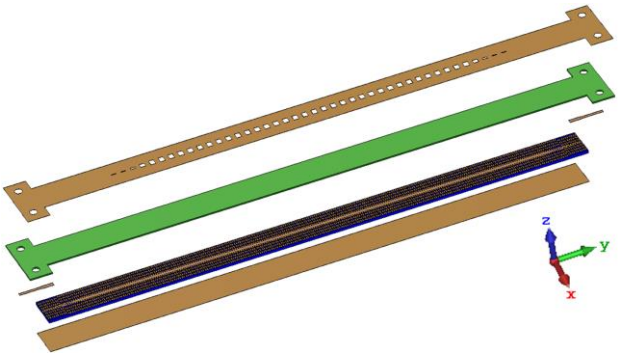

(b)

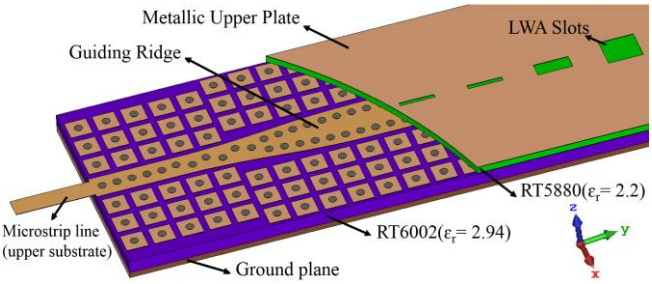

(c)

Fig. 10. (a) Total structure of the SIGW-LWA, (b) Separated view of the stacked layers, and (c) A zooming close to the MS line with the removed part of the upper substrate.

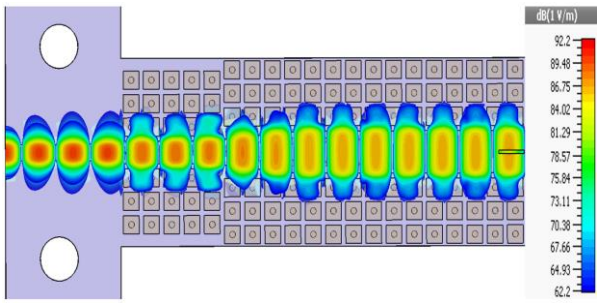

Fig. 11. Field distribution of the SIGW-LWA shown in Fig. 10.

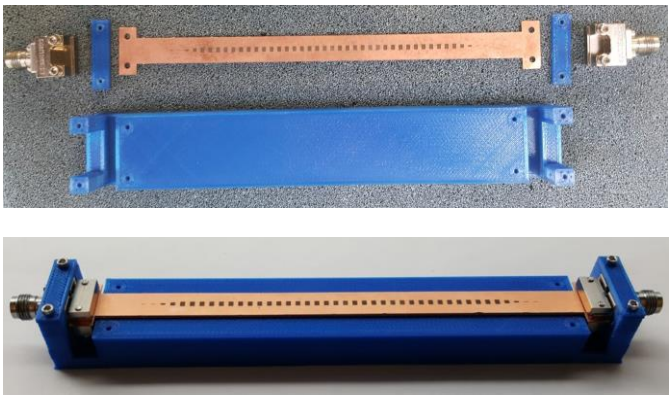

Fig. 12. Fabricated prototype of SIGW-LWA with 3D printed holder.

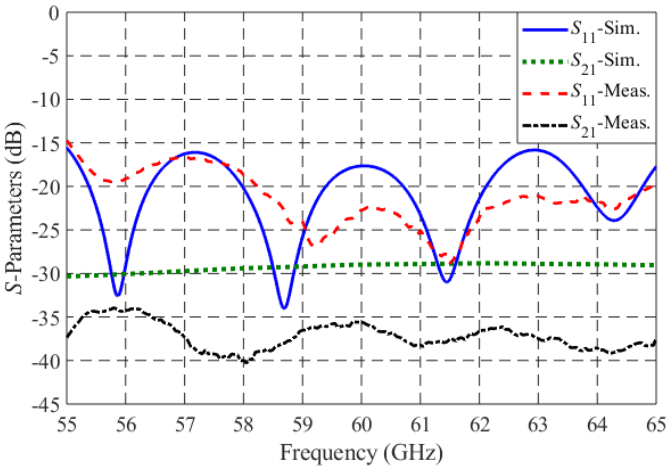

Fig. 13. Measured and simulated *S*-parameters of SIGW-LWA shown in Fig.10.

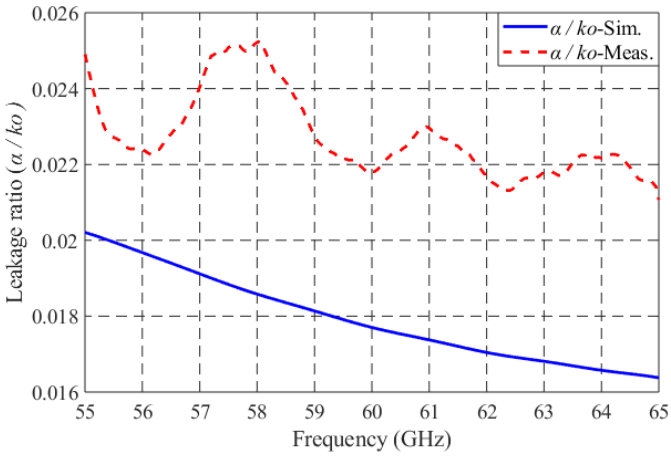

Fig. 14. Measured and simulated leakage ratio of the SIGW-LWA shown in Fig. 10.

Since the operating frequency band is 57 to 64 GHz, the antenna beam scanning range is -36° to -15°. However, if the entire possible operating bandwidth of the antenna is considered (52 to 68 GHz), the beam scanning would be from -62° to -5 in which the gain variation is less than 2 dB. Fig. 18 shows the *S*-parameters and the gain of the SIGW-LWA over the whole operating frequency band.

VI. SIGW-LWA Array

A. Power Divider Design

To design any array of this LWA, a power divider should be used. Here, the performance of a 2×1 array is investigated. A Y-shaped power divider is designed to feed SIGW-LWA arms, which is shown in Fig. 19. The same periodic structure of the SIWG-LWA with the same cell configuration given in Fig. 1 is used in the design of the power dividing circuit. The upper substrate and metal top plate are not shown in Fig. 19. The SIGW power divider arms are designed to match 50 Ω, and they are excited with the 50 Ω MS lines with the width of w_0 = 0.74 mm on the Rogers RT5880 substrate with ε_r = 2.2. Since the SIGW line and MS line have different propagation environments, the 50 Ω line of SIGW is achieved with the width of w_1 = 1 mm. A quarter-wavelength transformer with a characteristic impedance of 35.3 Ω is applied to match the 50 Ω line with the arms of the Y-shape power divider. The length and width of a quarter-wavelength transformer are l_2 = 1.9 mm, and w_2 = 1.52 mm, respectively. Fig. 20 shows the simulated *S*-parameters of the power divider. S_{11} is below -15 dB over the whole frequency band and the insertion loss is around 3.35 dB.

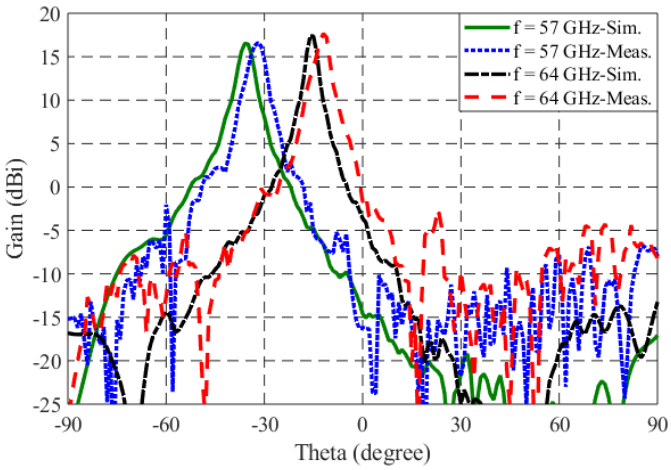

Fig. 15. Comparison between the measured and simulated realized gain of the co-polar E-plane radiation pattern at 57 GHz and 64 GHz.

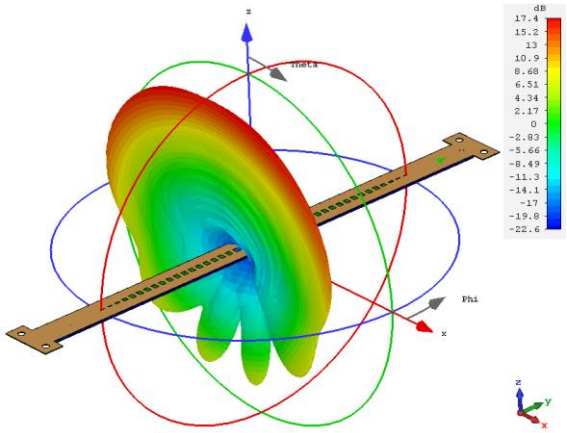

Fig. 16. Simulated 3D radiation pattern of the SIGW-LWA at 64 GHz.

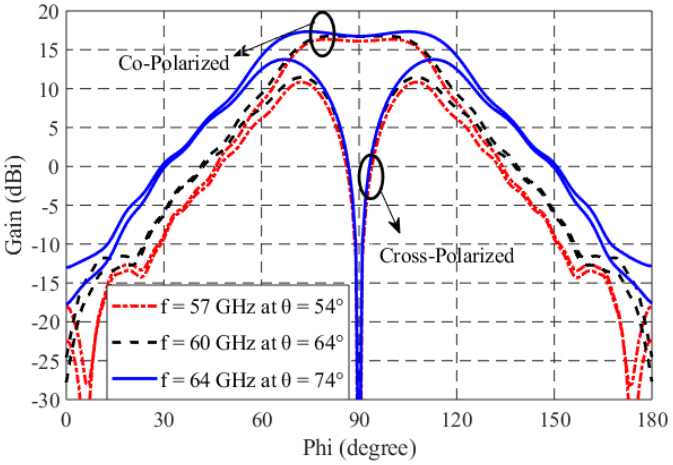

Fig. 17. Simulated co- and cross-polar H-plane radiation patterns at three frequencies, 57 GHz, 60 GHz and 64 GHz at θ = 54°, θ = 64°, and θ = 74°, respectively of the antenna in Fig. 9.

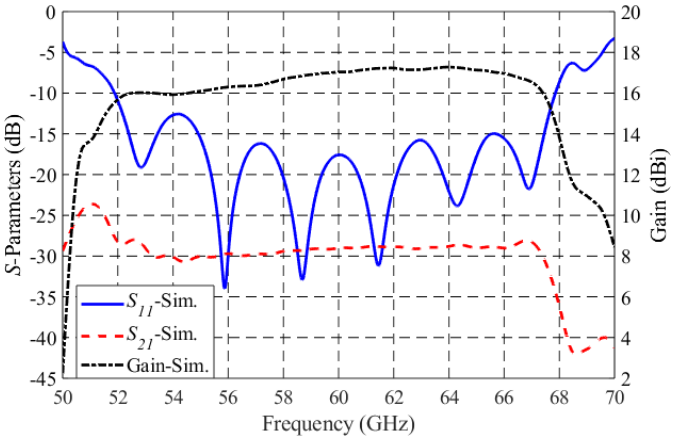

Fig. 18. Simulated S-parameters and gain of the SIGW-LWA.

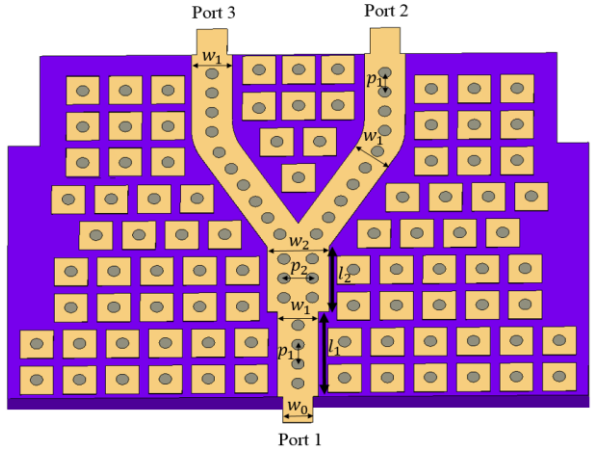

Fig. 19. Schematic of the Y-shape power divider (p_1 = 0.56mm, p_2 = 0.89mm, w_1 = 1mm, w_2 = 1.52mm, w_3 = 0.74mm, l_1 = 2.46mm, l_2 = 1.9mm).

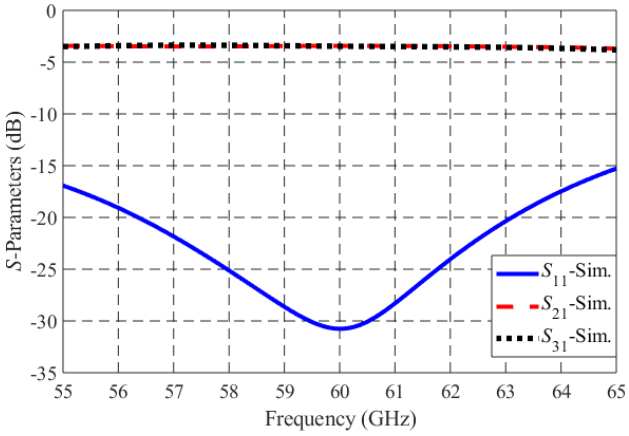

Fig. 20. Simulated *S*-parameters of the Y-shape power divider.

B. Array Design

In order to avoid the appearance of grating lobes, the distance between the two subarrays is less than λ_0 [37]. Two arms of the Y-shape power divider are extended to connect LWA subarrays as shown in Fig. 21(a). In this design, the same power divider is used on the other side of the array to connect the array to a single match load. Since the width of the SIGW ridgelines under the periodic slots are wider than the 50 Ω line, after the power divider section two rows of periodic cells are placed between the lines. Simulated *S*-parameters of the array are plotted in Fig. 23 showing a reflection coefficient below -10 dB in the operating frequency band. Such as single LWA, the array design also has a low and constant leakage ratio over the band supporting narrow beam radiation and long effective aperture.

As the LWA length is long enough ($20\lambda_0$) to radiate more than 90% of the power, just a little power remains at the end of the array. Therefore, instead of using another power divider for the matched load termination, the ends of subarrays are connected through a curved ridgeline, as shown in Fig. 21(b). In this way, the propagation wave at the end of each LWA sees the same characteristic impedance of SIGW line. In other words, instead of using two matched loads at the end of each subarray, we use each single array connected in series to act as a matched load for the other one. In addition, by this termination, the total length of the antenna decreases around $6\lambda_0$. Generally, by connecting the ends of the two arms the remaining power from each arm contributes to a higher side lobe in the forward direction, in the location of a possible main beam in the forward direction, with a level that depends on the percentage power remaining. However, if the length of the bend is tuned to be an odd multiple of half wavelength, the traveling waves at the end of each subarray receive 180° phase shift when reaches to the other side. Accordingly, instead of radiating as a forward beam, the remaining power at the end of each arm adds constructively to the main traveling power of the opposite side. Therefore, a slight gain increment could be expected compared to the matched array. It should be noticed that the length of the bend termination in the present design is set for 60.5 GHz, and its corresponding effect happens exactly at this frequency, but it also causes the mitigation of the forward beam at the other frequencies. Since the aperture length of the proposed LWA is long enough to

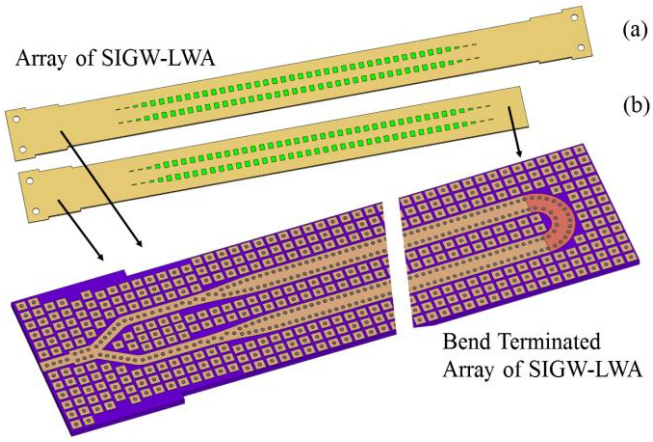

Fig. 21. Configuration of (a) Array of SIGW-LWA, and (b) Bend terminated array of SIGW-LWA.

have most of the power radiated. Therefore, having an open end may not affect the array radiation pattern considerably. However, in the case of shorter arrays, in which a stronger remaining power exists at the end of the arms, the bend termination could be a relatively appropriate and inexpensive solution to maximize the gain and minimize the emerging unwanted radiating lobes. The bend terminated array design is chosen for fabrication as shown in Fig. 22 with the 3D-printed holder. The simulated and measured *S*-parameters of this array is also plotted in Fig. 23. The simulated reflection coefficients of bend terminated array and matched load terminated array are the same, and both are below -10 dB over the operating band. There is also a good agreement between the simulated and measured results. Fig. 24 shows the simulated and measured co-polar E-plane radiation pattern of the bend terminated array at 60.5 GHz compared with the matched load terminated array, and the open-end terminated array. As can be seen, the reflected small portion of the power increases the sidelobe at a position of the possible beam if the input signal is provided from the opposite direction, which would have a higher level in the case of a shorter array; this, in fact, highlights the advantages of the bend connection. As shown, the bend terminated array radiation at this frequency is very close to the array with the matched load termination without any secondary minor forward beam, which means that the remaining power at the end of each arm constructively contributes to the other arm. Fig. 25 shows the simulated and measured realized gain of the co-polar E-plane radiation pattern of the bend terminated array at two different frequencies, 57 and 64 GHz, and they are compared with the matched array. Both array antennas can achieve 3 dB gain increment due to the constructive coupling of the slots. As shown in Fig. 25, the level of the minor lobes in the forward quadrant is 20 dB below the peak of the main beam within the entire band. The cross-polar E-plane patterns for all frequencies are -27 dB below main beam peak, and they are not shown in Figs. 24 and 25. A small shift in the beam direction is observed between simulated and measured radiation patterns, which may be due to the fabrication tolerances. Fig. 26 shows the realized gain, radiation efficiency, and total efficiency for both antenna arrays, and the single element of SIGW-LWA. The measured peak gain of the bend terminated array is 21.5 dBi with less than 1.3 dB variation and -15 dB sidelobe level. The beam scanning range of the proposed array is from –35˚ to –15˚ in the frequency

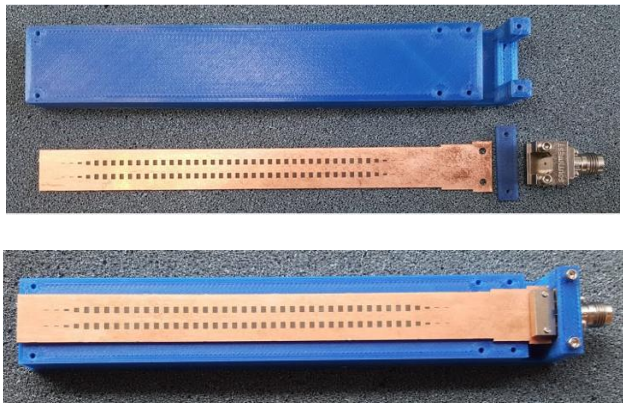

Fig. 22. Fabricated prototype of SIGW-LWA array with bend termination.

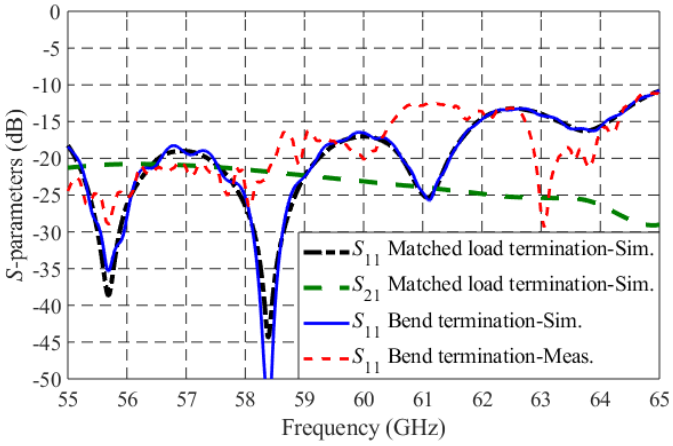

Fig. 23. Measured and simulated *S*-parameters of matched array and bend terminated array of SIGW-LWA.

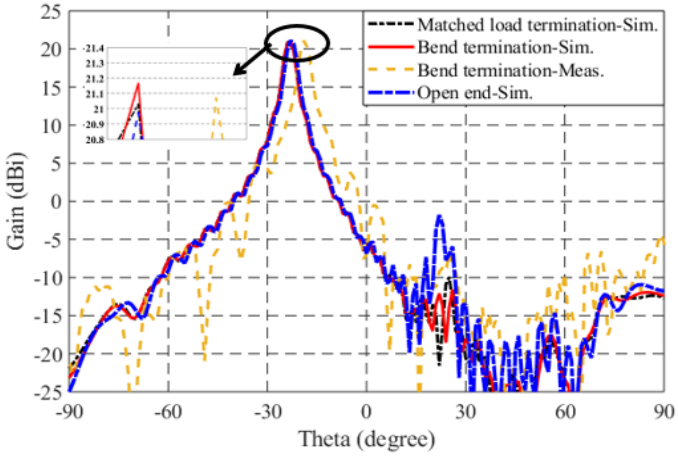

Fig. 24. Comparison between the measured and simulated realized gain of the co-polar E-plane radiation pattern of the matched array, bend terminated array and an open-ended array of SIGW-LWA at 60.5 GHz.

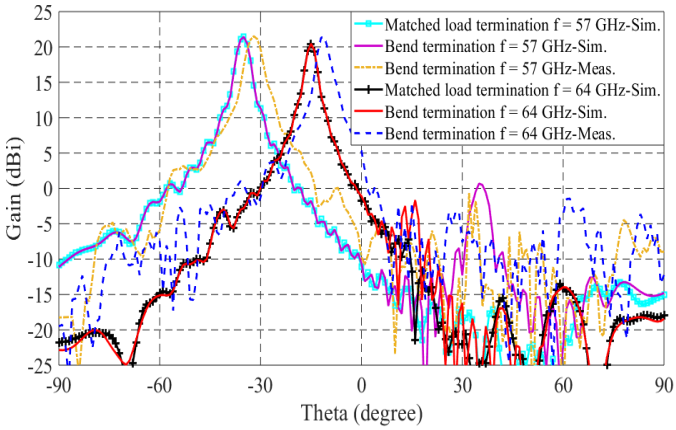

Fig. 25. Comparison between the measured and simulated realized gain of the co-polar E-plane radiation pattern of the matched array and bend terminated array of SIGW-LWA at 57 GHz and 64 GHz.

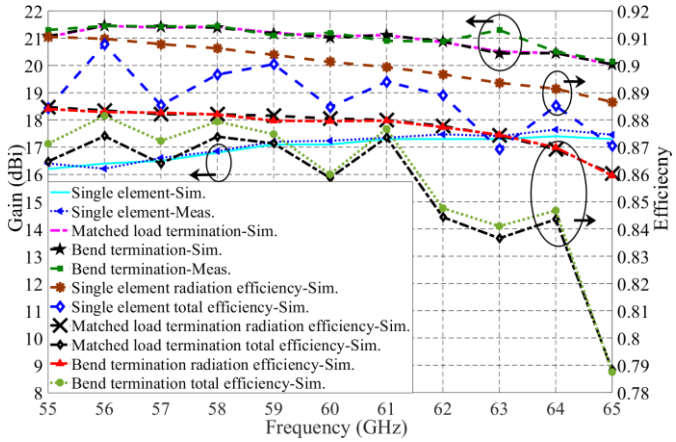

Fig. 26. Simulated and measured realized gain, radiation efficiency, and total efficiency of the single element, matched array and bend terminated array of SIGW-LWA.

Table. II
THE COMPARISON OF THE PROPOSED SIGW-LWA WITH OTHERS

Antenna	BW (%)	Gain (dBi)	Rad. Eff. (%)	length (λ_0)
SIGW-LWA (V-band)	27	17.67	89	28
Bend terminated array of SIGW-LWA(V-band)	23	21.5	87	29
SIW-LWA (X-band) [22]	22	12	70	12
MED-LWA (Ka-band) [38]	20	15.6	83	12
Dual-Beam DG-LWA (V-band) [39]	10	25 (F) 24(B)	-	58

range of 57-64 GHz. The radiation efficiency for both array antennas is more than 87% over the operating band. The total efficiency of the bend terminated array is more than 84%, which is a little higher than that of the matched array. Table. II shows a comparison between this work and others LWAs.

VII. CONCLUSIONS

Two designs of LWA based on the SIGW technology at the millimeter-wave band have been presented. The antennas have achieved almost constant high gain, high radiation efficiency with wide impedance bandwidth and fabricated with a low-cost multi-layered PCB technology. The single element of SIGW-LWA has shown 27% of bandwidth around the center frequency of 58.5 GHz and the measured peak gain of 17.67 dBi with less than 1.3 dB variation. Its radiation efficiency has reached more than 89% over the frequency range of 57-64 GHz. For the parallel-fed array, the ends of the array arms have been connected to each other providing shorter antenna length, and with the proper length of the connection (odd multiple of half wavelength), the remaining power on each arm has been utilized constructively in the radiation power. The bandwidth of the bend terminated array has reached 23% around the center frequency of 59 GHz with a measured peak gain of 21.5 dBi with less than 1.3 dB variation and -15 dB sidelobe level as well as 87% radiation efficiency. Good agreement between simulated and measured results of the single LWA and its array design has been observed.

REFERENCES

[1] S. Gong and M. Karlsson, "Pushing the Wireless Data Rate to the Internet Speed," *IEEE Access*, vol. 4, pp. 8787-8792, 2016.

[2] E. K. MacHale, G. Talli, and P. D. Townsend, "10 Gb/s bidirectional transmission in a 116 km reach hybrid DWDM-TDM PON," *2006 Optical Fiber Communication Conference and the National Fiber Optic Engineers Conference*, 2006, pp. 3 pp.

[3] H. Mopidevi. *et al.*,"Three-DimensionalMicrofabricated Broadband Patch Antenna for WiGig Applications," *IEEE Antennas and Wireless Propagation Letters*, vol. 13, pp. 828-831, 2014.

[4] P. S. Kildal, E. Alfonso, A. Valero-Nogueira and E. Rajo-Iglesias, "Local Metamaterial-Based Waveguides in Gaps Between Parallel Metal Plates," *IEEE Antennas and Wireless Propagation Letters*, vol. 8, pp. 84-87, 2009.

[5] P. S. Kildal, A. U. Zaman, E. Rajo-Iglesias, E. Alfonso and A. Valero-Nogueira, "Design and experimental verification of ridge gap waveguide in bed of nails for parallel-plate mode suppression," *IET Microwaves, Antennas & Propagation*, vol. 5, no. 3, pp. 262-270, Feb. 21, 2011.

[6] P. S. Kildal, A. A. Kishk and A. Tengs, "Reduction of forward scattering from cylindrical objects using hard surfaces," *IEEE Transactions on Antennas and Propagation*, vol. 44, no. 11, pp. 1509-1520, Nov 1996.

[7] E. Rajo-Iglesias and P. S. Kildal, "Numerical studies of bandwidth of parallel-plate cut-off realised by a bed of nails, corrugations and mushroom-type electromagnetic bandgap for use in gap waveguides," *IET Microwaves, Antennas & Propagation*, vol. 5, no. 3, pp. 282-289, Feb. 21, 2011.

[8] E. Pucci, A. U. Zaman, E. Rajo-Iglesias, P. S. Kildal, and A. Kishk, "Study of Q-factors of ridge and groove gap waveguide resonators," *IET Microwaves, Antennas & Propagation*, vol. 7, no. 11, pp. 900-908, August 20, 2013.

[9] H. Raza, J. Yang, P. S. Kildal and E. Alfonso Alós, "Microstrip-Ridge Gap Waveguide–Study of Losses, Bends, and Transition to WR-15," *IEEE Transactions on Microwave Theory and Techniques*, vol. 62, no. 9, pp. 1943-1952, Sept. 2014.

[10] N. Bayat-Makou and A. A. Kishk, "Millimeter-Wave Substrate Integrated Dual Level Gap Waveguide Horn Antenna," *IEEE Transactions on Antennas and Propagation*, vol. 65, no. 12, pp. 6847-6855, Dec.2017.

[11] F. Sadjadi, M. Helgeson, M. Radke, and G. Stein, "Radar synthetic vision system for adverse weather aircraft landing," *IEEE Transactions on Aerospace and Electronic Systems*, vol. 35, no. 1, pp. 2-14, Jan 1999.

[12] S. Gu, C. Li, X. Gao, Z. Sun and G. Fang, "Terahertz Aperture Synthesized Imaging With Fan-Beam Scanning for Personnel Screening," *IEEE Transactions on Microwave Theory and Techniques*, vol. 60, no. 12, pp. 3877-3885, Dec. 2012.

[13] Young-Jin Park and W. Wiesbeck, "Offset cylindrical reflector antenna fed by a parallel-plate Luneburg lens for automotive radar applications in millimeter-wave," *IEEE Transactions on Antennas and Propagation*, vol. 51, no. 9, pp. 2481-2483, Sep 2003

[14] C. H. Walter, *Traveling Wave Antennas*, McGraw-Hill, New York, 1965.

[15] Yu-Chiao Chen, Ching-Kuo Wu, and C. K. C. Tzuang, "Dual-frequency electric-magnetic-electric microstrip leaky-mode antenna of a single fan beam," *IEEE Transactions on Microwave Theory and Techniques*, vol. 50, no. 12, pp. 2713-2720, Dec 2002.

[16] L A. A. Oliner and D. R. Jackson, Leaky-wave antennas, in Antenna Engineering Handbook, 4th Ed., J. L. Volakis (Ed.), McGraw-Hill, New York, 2007, Chap. 11.

[17] A. Mallahzadeh and S. Mohammad-Ali-Nezhad, "Periodic Collinear-Slotted Leaky Wave Antenna with Open Stopband Elimination," *IEEE Transactions on Antennas and Propagation*, vol. 63, no. 12, pp. 5512-5521, Dec. 2015.

[18] Y. Lyu *et al*., "Leaky-Wave Antennas Based on Noncutoff Substrate Integrated Waveguide Supporting Beam Scanning from Backward to Forward," *IEEE Transactions on Antennas and Propagation*, vol. 64, no. 6, pp. 2155-2164, June 2016.

[19] Y. Dong and T. Itoh, "Composite Right/Left-Handed Substrate Integrated Waveguide and Half Mode Substrate Integrated Waveguide Leaky-Wave Structures," *IEEE Transactions on Antennas and Propagation*, vol. 59, no. 3, pp. 767-775, March 2011.

[20] Nasimuddin, Z. N. Chen and X. Qing, "Multilayered Composite Right/Left-Handed Leaky-Wave Antenna with Consistent Gain," *IEEE Transactions on Antennas and Propagation*, vol. 60, no. 11, pp. 5056-5062, Nov. 2012.

[21] W. Cao, Z. N. Chen, W. Hong, B. Zhang, and A. Liu, "A Beam Scanning Leaky-Wave Slot Antenna With Enhanced Scanning Angle Range and Flat Gain Characteristic Using Composite Phase-Shifting Transmission Line," *IEEE Transactions on Antennas and Propagation*, vol. 62, no. 11, pp. 5871-5875, Nov. 2014.

[22] J. Liu, D. R. Jackson, and Y. Long, "Substrate Integrated Waveguide (SIW) Leaky-Wave Antenna With Transverse Slots," in *IEEE Transactions on Antennas and Propagation*, vol. 60, no. 1, pp. 20-29, Jan. 2012.

[23] N. Yan, K. Ma, H. Zhang, and Z. Jian, "A Novel Substrate Integrated Suspended Line Wideband Leaky-Wave Antenna," IEEE Antennas and *Wireless Propagation Letters*, vol. 16, pp. 2642-2645, 2017.

[24] N. Nasimuddin, Z. N. Chen and X. Qing, "Substrate Integrated MetamaterialSingle-substrate integration technique of planar circuits and w-Based Leaky-Wave Antenna With Improved Boresight Radiation Bandwidth," *IEEE Transactions on Antennas and Propagation*, vol. 61, no. 7, pp. 3451-3457, July 2013.

[25] Y. Mohtashami and J. Rashed-Mohassel, "A Butterfly Substrate Integrated Waveguide Leaky-Wave Antenna," *IEEE Transactions on Antennas and Propagation*, vol. 62, no. 6, pp. 3384-3388, June 2014.

[26] Y. Lyu, F. Meng, G. Yang, Q. Wu and K. Wu, "Leaky-Wave Antenna With Alternately Loaded Complementary Radiation Elements,"*IEEE Antennas and Wireless Propagation Letters*, vol. 17, no. 4, pp. 679-683, April 2018.

[27] E. Rajo-Iglesias and P. S. Kildal, "Numerical studies of bandwidth of parallel-plate cut-off realised by a bed of nails, corrugations and mushroom-type electromagnetic bandgap for use in gap waveguides," *IET Microwaves, Antennas & Propagation*, vol. 5, no. 3, pp. 282-289, Feb. 21, 2011.

[28] N. Bayat-Makou and A. A. Kishk, "Realistic Air-Filled TEM Printed Parallel-Plate Waveguide Based on Ridge Gap Waveguide," IEEE Transactions on Microwave Theory and Techniques, vol. 66, no. 5, pp. 2128-2140, May 2018.

[29] D. Deslandes and Ke Wu, "Single-substrate integration technique of planar circuits and waveguide filters," *IEEE Transactions on Microwave Theory and Techniques*, vol. 51, no. 2, pp. 593-596, Feb. 2003.

[30] C. Caloz, T. Itoh and A. Rennings, "CRLH metamaterial leaky-wave and resonant antennas," *IEEE Antennas and Propagation Magazine*, vol. 50, no. 5, pp. 25-39, Oct. 2008.

[31] R. C. Johnson (Ed.), Antenna Engineering Handbook, Third Edition, New York, McGraw Hill, 1992, Chapter 10.

[32] Constantine A. Balanis, "Microstrip and Mobile Communications Antennas" *Antenna Theory Analysis and Design*, 1, Wiley Telecom, pp.841.

[33] M. Sharifi Sorkherizi, A. Dadgarpour, and A. A. Kishk, "Planar High-efficiency Antenna Array Using New Printed Ridge Gap Waveguide Technology," *IEEE Transactions on Antennas and Propagation*, vol. 65, no. 7, pp. 3772-3776, July 2017.

[34] M. Sharifi Sorkherizi and A. A. Kishk, "Self-Packaged, Low-Loss, Planar Bandpass Filters for Millimeter-Wave Application Based on Printed Gap Waveguide Technology," *IEEE Transactions on Components, Packaging and Manufacturing Technology*, vol. 7, no. 9, pp. 1419-1431, Sept. 2017.

[35] Constantine A. Balanis, "Leaky-Wave Antennas," *Modern Antenna Handbook* , 1, Wiley Telecom, pp.338.

[36] F. Mesa, C. di Nallo, and D. R. Jackson, "The theory of surface-wave and space-wave leaky-mode excitation on microstrip lines," *IEEE Transactions on Microwave Theory and Techniques*, vol. 47, no. 2, pp. 207-215, Feb 1999.

[37] Constantine A. Balanis, "Arrays: Linear, Planar, and Circular" *Antenna Theory Analysis and Design*, 1, Wiley Telecom, pp.298.

[38] K. M. Mak, K. K. So, H. W. Lai and K. M. Luk, "A Magnetoelectric Dipole Leaky-Wave Antenna for Millimeter-Wave Application," *IEEE Transactions on Antennas and Propagation*, vol. 65, no. 12, pp. 6395-6402, Dec. 2017.

[39] Z. L. Ma, K. B. Ng, C. H. Chan, and L. J. Jiang, "A Novel Supercell-Based Dielectric Grating Dual-Beam Leaky-Wave Antenna for 60-GHz Applications," *IEEE Transactions on Antennas and Propagation*, vol. 64, no. 12, pp. 5521-5526, Dec. 2016.

Mohammad Reza Rahimi received his M.Sc. degree in electrical and computer engineering from Concordia University, Montréal, QC, Canada, in 2018. From 2017 to 2018, he was with Laboratory of Advanced Technology on Antenna and Microwave Systems (LATAMS) at Concordia University and he was a Research and Teaching Assistant with Concordia University from 2015 to 2018. In 2018, he joined Poly-Grames Research Center at Polytechnique Montréal (University of Montréal) where he is currently pursuing toward his Ph.D. degree. His research interests include Massive MIMO antenna, Hybrid smart antenna beamforming, Butler matrices, leaky-wave antennas and adaptive smart antennas. His paper was awarded as a finalist at 2018 IEEE AP-S/URSI conference. He has served as a Reviewer for 2019 IEEE AP-S/URSI.

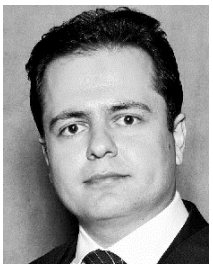

Nima Bayat-Makou (S'14–M'18) received the Ph.D. degree in electrical and computer engineering from Concordia University, Montréal, QC, Canada, in 2017**.** From 2013 to 2017, he was a Research and Teaching Assistant with Concordia University. He is currently a Postdoctoral Scholar with Poly-Grames Research Center, Polytechnique Montréal (University of Montréal). He has authored several referred journal articles and conference papers and holds two patents. His research interests include millimeter-wave antennas and waveguides based on substrate integrated technologies, electromagnetic bandgap structures and surfaces, active antenna arrays, massive MIMO subarrays and leaky-wave antennas.

Dr. Bayat-Makou was a recipient of the Natural Sciences and Engineering Research Council of Canada (NSERC) and the Fonds de recherche du Québec – Nature et technologies (FRQNT) Postdoctoral Fellowships, the International Union of Radio Science (URSI) Young Scientist Award, and the Second Prize of 2017 STARaCom competition. He has served as a Reviewer for IEEE AP-S and MTT-S journals and magazine.

Ahmed A. Kishk (F'98) received the B.S. degree in electronic and communication engineering from Cairo University, Cairo, Egypt, in 1977, the B.Sc. degree in applied mathematics from Ain Shams University, Cairo, in 1980, and the M. Eng. and Ph.D. degrees from the Department of Electrical Engineering, University of Manitoba, Winnipeg, MB, Canada, in 1983 and 1986, respectively. In 1986, he joined the Department of Electrical Engineering, the University of Mississippi, Oxford, MS, USA, where he was a Professor. He offered several short courses in international conferences. Since 2011, he has been the Tier 1 Canada Research Chair of Advanced Antenna Systems with Concordia University, Montreal, QC, Canada, where he is currently a Professor. He has authored over 330 refereed journal articles and 450 conference papers. He has co-authored four books and several book chapters and edited three books. His current research interests include the areas of millimeter-wave antennas for 5G applications, analog beamforming network, dielectric resonator antennas, microstrip antennas, small antennas, microwave sensors, RFID antennas for readers and tags, multifunction antennas, microwave circuits, EBG, artificial magnetic conductors, soft and hard surfaces, phased array antennas, and computer-aided design for antennas, reflect/transmit array, wearable antennas, and feeds for parabolic reflectors. Dr. Kishk is a Fellow of the Applied Computational Electromagnetics Society and of the Electromagnetic Academy in recognition of contributions and continuous improvements to teaching and research to prepare students for future careers in antennas and microwave circuits. He is a member of the IEEE Antennas and Propagation Society, Microwave Theory and Techniques Society, Sigma Xi Society, the U.S. National Committee of International Union of Radio Science Commission B, Phi Kappa Phi Society, Electromagnetic Compatibility Society, and Applied Computational Electromagnetics Society. He was the 2017 AP-S President. He was a Technical Program Committee member for several international conferences. He was a member of the AP AdCom from 2013 to 2015. He was a recipient of several awards, including the 1995 and 2006 Outstanding Paper Award for papers published in the Applied Computational Electromagnetic Society Journal, the 1997 Outstanding Engineering Educator Award from the Memphis Section of the IEEE, the Outstanding Engineering Faculty Member of the Year in 1998 and 2009, the Faculty Research Award for outstanding performance in research in 2001 and 2005, the Award of Distinguished Technical Communication for an entry in the IEEE Antennas and Propagation Magazine in 2001, the Valued Contribution Award for Outstanding Invited Presentation—EM Modeling of Surfaces with STOP or GO Characteristics—Artificial Magnetic Conductors and Soft and Hard Surfaces—from the Applied Computational Electromagnetic Society, the IEEE Microwave Theory and Techniques Society Microwave Prize in 2004, and the 2013 Chen-To Tai Distinguished Educator Award of the IEEE Antennas and Propagation Society. He was an Associate Editor of IEEE Antennas and Propagation Magazine from 1990 to 1993. He was a Distinguished Lecturer of the IEEE Antennas and Propagation Society from 2013 to 2015. He was an Editor of IEEE Antennas and Propagation Magazine from 1993 to 2014. He was a Guest Editor of the "Special Issue on Artificial Magnetic Conductors, Soft/Hard Surfaces, and Other Complex Surfaces" of the IEEE TRANSACTIONS ON ANTENNAS AND PROPAGATION in 2005.